Eur. Phys. J. Special Topics **219**, 3–12 (2013)

DOI: 10.1140/epjst/e2013-01775-5

THE EUROPEAN PHYSICAL JOURNAL SPECIAL TOPICS

Regular Article

Two-dimensional steady states in off-critical mixtures with high interface tension

F.A.M. Bribesh[1,2], S. Madruga[3,a] and U. Thiele[1]

[1] Department of Mathematical Sciences, Loughborough University, Loughborough, Leicestershire, LE11 3TU, UK
[2] Department of Mathematics, Zawia University, Zawia, Libya
[3] ETSI Aeronáuticos, Universidad Politécnica de Madrid, Plaza Cardenal Cisneros 3, 28040 Madrid, Spain

Received 1 July 2012 / Received in final form 18 January 2013
Published online xx February 2013

Abstract. We present 2D steady concentration profiles of confined layers of off-critical polymer blends. The layer rests on a solid substrate and has a flat free surface due to very high surface tension. The profiles correspond to non-linear steady solutions of the Cahn-Hilliard equation in a rectangular domain. The free polymer-gas interface is considered to be sharp, while the internal interfaces are diffuse. We explore the rich solution structure (including laterally structured layers, stratified layers, checkerboard structures, oblique states and droplets) as a function of mean concentration.

1 Introduction

Binary fluid mixtures are fluids that consist of two chemical species. Polymer blends are an example that is often investigated due to their industrial interest and typical slow evolution times suitable for experimental analysis [1]. The blends appear either in a mixed homogeneous state, or in various phase separated states with interfaces separating the phases, depending on the average composition and temperature. At large scales the interface between two phases can be modeled with great success by a sharp interface, however at the micro- and nanoscale the width of the interface can be comparable to the dimensions of a possible external confinement or film thickness of the mixture. Therefore an appropriate modelling of the diffuse interface is important. The Cahn-Hilliard equation [2,3] represents a phase field model based on thermodynamic principles that gives the diffusive evolution of the composition field as divergence of a flux that itself results as the gradient of the chemical potential for binary mixtures with diffuse interfaces. Coupling this equation to a transport equation for momentum (Navier-Stokes with stress tensor that contains Korteweg stresses) the so-called model-H results that allows for a study of transport processes by diffusion and convection (see [4] and references therein). For confined layers of binary blends, such models have been used to study the stability of homogeneous blends

[a] e-mail: santiago.madruga@upm.es

with respect to purely diffusive [5,6] and coupled diffusive and convective modes [7] predicting, e.g., the occurrence of surface modes of spinodal decomposition [5].

Previously we re-derived model-H, compared and consolidated several versions existing in the literature, and supplemented it by coupled boundary conditions for momentum and concentration at the free surface of a film on a solid substrate [8]. A study of steady homogeneous and layered films [8] and of their linear stability [9] at critical composition (identical mean concentration for both components) followed that showed qualitative differences between purely diffusive and coupled diffusive and convective instability modes. However, laterally structured films and more complicated states, e.g., with oblique diffuse interfaces, are possible and are for critical composition studied in Ref. [10] by determining steady solutions of the Cahn Hilliard equation in rectangular domains and also with a deformable free surface. Furthermore we distinguished the cases without and with energetic bias at the free surface. Refs. [8–10] set our study in the context of the experimental literature, the literature on model-H, and on some one-dimensional mathematical results for the Cahn-Hilliard equation [11,12]. However, regrettably we missed to point out connections to later relevant mathematical work on solutions of the Cahn Hilliard equation, in particular, for two-dimensional square domains. In particular, [13] studies the stability of linear modes on the plane for the Cahn-Hilliard equation at critical concentration and the geometry of the nodal domains of doubly periodic states, Refs. [14,15] investigate critical points of the energy underlying the Cahn-Hilliard equation on a square domain in dependence of the mean concentration, their Figs. 6.1 sketch some solution branches in dependence of mean concentration that are similar to primary branches discussed below for a rectangular domain; one-dimensional solutions are discussed in [16]. Finally, Refs. [17,18] analyses the fine structure of the global attractor of the Cahn-Hilliard equation on the square analytically and numerically. For instance, they discuss bifurcation diagrams with the system size [17] and mean concentration [18] as control parameter, similar to our analysis of rectangular domains in the non-biased flat free surface critical [10] and off-critical (present work) case. Because of the different domain geometry we are not able to compare bifurcation diagrams directly. We also note that to our knowledge no results exist in the mathematical literature for the cases of energetic bias at the free surface, a modulated free surface, or a combination of both. Such states are discussed at length in Ref. [10] in the critical case (mean concentration zero). The present consideration of a rectangular geometry without energetic bias and flat free surface in the off-critical case will serve as a reference case for a future study of the off-critical case with energetic bias at the free surface and with modulated free surface.

Here we extend the results Ref. [10] gave for flat films at critical concentration towards off-critical compositions, a case very relevant in experiments since there a balanced overall composition of the two species is actually an exception. In particular, we study steady nonlinear solutions of the Cahn-Hilliard equation (as the steady limit of model-H) for layers of fixed rectangular geometry. This represents a preliminary step for a study of the off-critical case for a deformable free surface. We analyse layered films, laterally structured states, oblique structures, and checkerboard states.

2 Model equations

We study steady solutions of the Cahn-Hilliard equation [2,3] for films on bounded domains. In particular, we obtain nonlinear solutions by numerically minimising the Lyapunov functional

$$F(h,c) = \frac{1}{L}\int_0^L \left\{ \gamma\sqrt{1+(\partial_x h)^2} + \int_0^{h(x)} \left[\frac{1}{2}(\nabla c)^2 + f(c)\right] dz \right\} dx \qquad (1)$$

where L is the lateral length of the film, H is the mean film thickness, and $h(x)$ is the local film height. A cartesian frame is used with origin at the left bottom corner of the film. Here, the free surface and substrate are considered to be energetically neutral and flat. For results with energetic surface bias and/or a modulated free surface in the critical case see Ref. [10]. We use $f = \frac{1}{4}(1-c^2)^2$ for the local free energy, where $c = c_1 - c_2$ with $c_{1,2}$ the volume fractions of each component of the mixture. To characterise the non linear solutions we use the L_2-norm of the concentration field, defined as $||\delta c|| = \sqrt{1/(L\,H)\int_0^L \int_0^{h(x)} \left(c(x,z)-\bar{c}\right)^2 dz dx}$, where $\bar{c}$ is the mean concentration.

The value of the surface tension γ determines the deformability of the free surface. For small γ the surface can undergo strong surface deflections [10]. Here we employ a very high value ($\gamma = 1000$) to guarantee a flat film of constant height $h(x) = H$.

The energy functional is minimised using a Newton gradient method and a spatial discretization based on finite elements. In particular, the domain has been discretised with linear triangular elements using a natural isoparametric coordinate system and an adaptive grid [19]. No flux boundary conditions are used at all boundaries. The resulting variational problem is numerically solved allowing us to obtain the concentration profile inside the film. For details see Ref. [10].

3 Linear stability

To determine the linear stability of homogeneous layers $c(x,z) = \bar{c}$ we impose infinitesimal fluctuations of the form $\sim \exp(ik_x x + ik_z z + \beta t)$. Considering only modes that fit the rectangular domain results in discrete lateral and vertical wave numbers $k_x = 2\,\pi\,s/L$ with mode number $s = 0, 1/2, 1, \ldots$ and $k_z = 2\,\pi\,n/H$ with mode number $n = 0, 1/2, 1, \ldots$, respectively. Linearizing the Cahn-Hilliard equation about $\bar{c}$ one obtains the dispersion relation $\beta = -(k_x^2 + k_z^2)\left[k_x^2 + k_z^2 + 3\,\bar{c}^2 - 1\right]$. The film is unstable ($\beta > 0$) for modes with $k_x^2 + k_z^2 < 1 - 3\,\bar{c}^2$. The various modes result in different concentration thresholds of instability (at $\beta = 0$). For mode numbers (s, n) one has

$$\bar{c}_{s,n} = \frac{1}{\sqrt{3}}\sqrt{1 - \left(\frac{2\pi s}{L}\right)^2 - \left(\frac{2\pi n}{H}\right)^2} \tag{2}$$

Note that an infinite system becomes linearly unstable to a long wave mode $k_x = k_y = 0$ at $\bar{c}_{\rm sp} = 1/\sqrt{3}$ (spinodal line).

Note that all critical concentrations $\bar{c}_{s,n}$ (Eq. (2)) also correspond to loci of pitchfork bifurcations where branches of structured solutions bifurcate from the trivial homogeneous solution. For instance, for $H = 5$ and $L = 12$ when decreasing $\bar{c}$ one finds that the first laterally structured, layered and checkerboard solutions emerge at $\bar{c}_{1/2,0} = 0.56$, $\bar{c}_{0,1/2} = 0.45$, and $\bar{c}_{1/2,1/2} = 0.42$, respectively.

Even if the binary mixtures are linearly stable they might be unstable with respect to finite size perturbations in a metastable region outside the spinodal line. The threshold for the infinite system (binodal line) also provides the coexisting concentrations and is derived from a Maxwell construction to be $c_{\rm bi} = \pm 1$.

4 Steady solutions in 2D

Next we study the 2D non linear solutions for films of polymer blends of thickness $H = 5$ and lateral extension $L = 12$. The free surface is imposed to be flat.

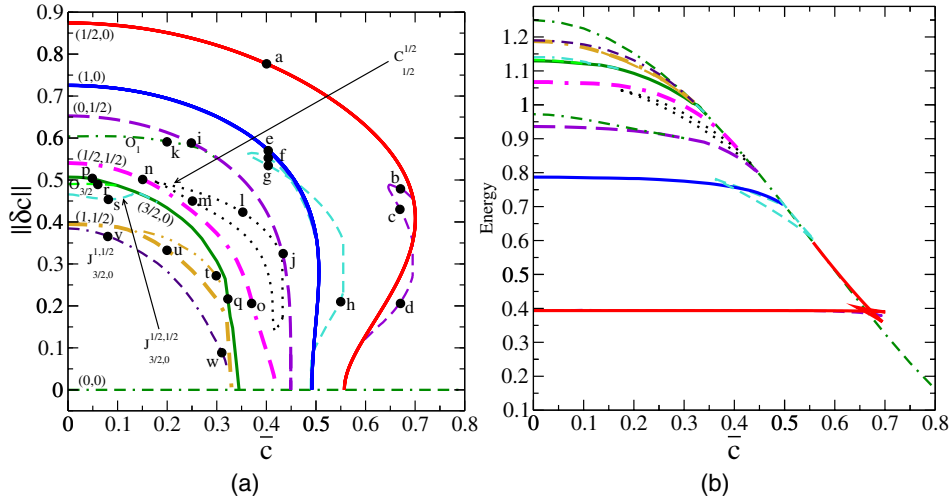

Fig. 1. (colour online) Shown are for confined films of height $H = 5$ and lateral domain size $L = 12$ as a function of mean concentration $\bar{c}$ (a) the L_2-norm of the concentration field and (b) the energy $E = F - \gamma$, where we subtracted the constant offset γ. We indicate laterally stratified films as heavy solid lines (cf. Sect. 4.1); checkerboard films as dash-dotted lines (cf. Sect. 4.3); layered films as heavy dashed lines (cf. Sect. 4.2). Oblique films are marked by O labels (cf. Sect. 4.4); oblique checkerboard states by J labels (cf. Sect. 4.5); and droplet and stripe states by C label (cf. Sect. 4.6).

4.1 Laterally structured films

We find three branches of laterally structured films: $(1/2, 0)$, $(1, 0)$ and $(3/2, 0)$, shown as heavy solid lines in Fig. 1. At concentration $\bar{c} = 0$ (critical case) they correspond to vertically homogeneous films with lateral modulations of periods $2\,L$, L and $2/3\,L$, respectively (cf. Ref. [10]). The L_2-norm on these branches is maximal at $\bar{c} = 0$. They join the homogeneous base state $(0, 0)$ at $\bar{c}_{1/2,0} = 0.56$ (subcritical), $\bar{c}_{1,0} = 0.49$ (supercritical), $\bar{c}_{3/2,0} = 0.36$ (supercritical), respectively, as also calculated from Eq. (2).

The branch $(1/2, 0)$ extends beyond the spinodal limit at $\bar{c}_{\rm sp} = 1/\sqrt{3}$ up to the saddle node at $\bar{c} \approx 0.7$. This is still far below the binodal at $c_{\rm bi} = 1$. The branches $(1, 0)$ and $(3/2, 0)$ remain well within the spinodal region. The branch $(3/2, 0)$ has no saddle node, i.e., the L_2-norm decays monotonously with $\bar{c}$.

Typical profiles from the $(1/2, 0)$, $(1, 0)$, and $(3/2, 0)$ branches are given in Figs. 3(a), 3(b), and 3(c), respectively. Following these branches towards the homogeneous state $(0, 0)$ the transition occurs through a widening of the internal diffuse interfaces. At $\bar{c} = 0$ all the profiles are invariant under a subgroup of the symmetries of the equation and boundary conditions (cf. caption of Fig. 2 and Ref. [10]). The number of symmetry elements is normally further reduced for off-critical compositions. In particular, we find for branch $(3/2, 0)$ the group $\{I, \sigma_{xc}, \pi_z, \rho_{xzc}\}$ at $\bar{c} = 0$ becomes $\{I, \sigma_{xc}\}$ at $\bar{c} \neq 0$; for branch $(1, 0)$ one has $\{I, \sigma_{xc}, \sigma_{zc}, \pi_c\} \longrightarrow \{I, \sigma_{xc}, \sigma_{zc}, \pi_c\}$; and for branch $(1/2, 0)$ the change is $\{I, \sigma_{xc}, \pi_z, \rho_{xyc}\} \longrightarrow \{I, \sigma_{xc}\}$.

Interestingly, when increasing $\bar{c}$ additional branches emerge from the $(s, 0)$ branches in further symmetry breaking pitchfork bifurcations. This occurs for the $(1/2, 0)$ and $(1, 0)$ branch at $\bar{c} = 0.69$ and $\bar{c} = 0.48$, respectively. On the new branches the vertical interfaces incline rightwards, in such a way that the three-phase contact region at the substrate and at the free surface are shifted to the left and to the right, respectively. For the branch emerging from $(1/2, 0)$, this progressive shifts leads to the creation of a droplet in the right bottom corner, as shown in Figs. 3 and 3.

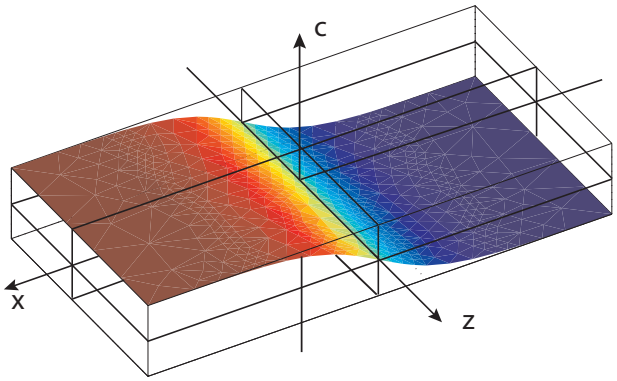

Fig. 2. (colour online) Sketch of a film presented in the space spanned by coordinates x, z and concentration c. The planes xz, xc and zc are perpendicular to the c, z and x axes, respectively. To characterise the symmetries of a solution in this space, we denote by I the identity transformation; by σ_{xz}, σ_{xc} and σ_{zc} the reflections at the planes xz, xc and zc, respectively; by π_x, π_z, π_c the rotation about x, z and c axes by π, respectively; and by ρ_{xzc} the inversion at the origin.

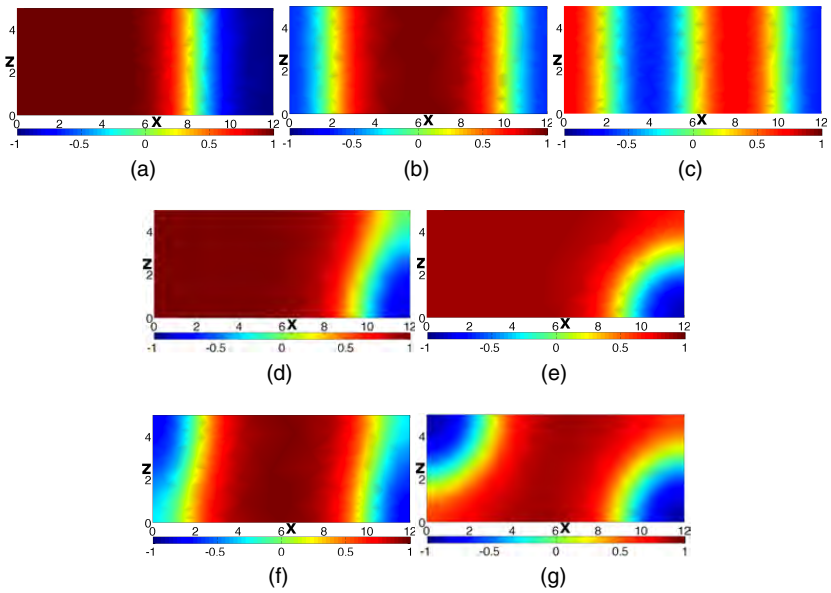

Fig. 3. Upper row: typical concentration profiles on the laterally structured branches at off-critical compositions: (a) $(1/2, 0)$, (b) $(1, 0)$, and (c) $(3/2, 0)$. The loci of these states in Fig. 1(a) are indicated by labels a, e, and p, respectively. Middle row: profiles on branch emerging from the branch $(1/2, 0)$ marked in Fig. 1(a) with the labels b and c. Lower row: profiles on branch emerging from the branch $(1, 0)$ marked in Fig. 1(a) with the labels f and g. Remaining parameters as in Fig. 1(a).

The new branch is only invariant under $\{I\}$. For $(1, 0)$, two droplets are formed – one in the right bottom and left upper corner each (Figs. 3f, 3g). The related branch is invariant under $\{I, \pi_c\}$.

The energy per unit of length of the three branches is compared in Fig. 1(b). Inside the spinodal region the homogeneous branch $(0, 0)$ has the largest energy. Actually, nearly everywhere in the binodal region the homogeneous state has for a given

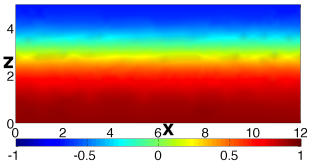

Fig. 4. Typical layered concentration profile on the branch $(0, 1/2)$, marked in Fig. 1(a) with the label *i*.

mean concentration a larger energy than all the phase separated states. The higher energy of the $(3/2, 0)$ branch, intermediate of $(1, 0)$ and lowest of the $(1/2, 0)$ branch is due to the number of internal diffusive interfaces, proportional to their energetic cost. Increasing $\bar{c}$ from zero, there is a progressive widening of the internal diffuse interfaces leading to smaller concentration gradients and therefore to a lower total energy. This is visible in Fig. 1(b) for all the branches as a slow monotonous decrease of the energy with $\bar{c}$.

Although a full analysis of the linear stability of the obtained solutions is out of our present scope we sketch conclusions obtained from the bifurcational and energetic structure observed in Figs. 1 and 1 at the example of the laterally structured branch $(1/2, 0)$ and its side branch: As shown in Sect. 3, the homogeneous state is linearly stable $\bar{c}_{1/2,0} > 0.56$ where it acquires an instability w.r.t. a lateral structuring. It is the branch of lowest energy above $\bar{c} = 0.67$. The branch $(1/2, 0)$ bifurcates subcritically, has one unstable eigenvalue before it acquires a second one at about $\bar{c} = 0.59$ where the side branch emerges. These two modes consecutively stabilise at the saddle node of the $(1/2, 0)$ branch at $\bar{c} = 0.70$ and at $\bar{c} = 0.696$ where the side branch ends again. Below $\bar{c} = 0.696$ the $(1/2, 0)$ branch is stable and corresponds to the branch of lowest energy. The side branch starts off supercritically at $\bar{c} = 0.59$ with one unstable mode, becomes stable at its first saddle-node at about $\bar{c} = 0.698$ (confirmed by the fact that it is the non-trivial branch of lowest energy between $\bar{c} = 0.668$ and 0.698), becomes unstable again at its second saddle-node at $\bar{c} = 0.65$ before it ends supercritically at $\bar{c} = 0.696$. Note that here we do not discus the stability of the other branches.

4.2 Layered films

Layered films of the type $(0, 1/2)$ are characterized by a single horizontal diffusive interface and only exist within the spinodal region (heavy dashed line in Fig. 1(a)). Its L_2-norm is maximal at $\bar{c} = 0$ and decreases monotonously with $\bar{c}$ until joining the homogeneous solution through a pitchfork bifurcation at $\bar{c}_{0,1/2} = 0.45$ as confirmed by Eq. (2).

Figure 4(a) shows a typical concentration profile on this branch. Increasing $\bar{c}$ widens the diffuse interface and brings it towards the substrate or the free surface, and leads to a continuous transition towards the homogeneous state. At $\bar{c} = 0$ this branch is invariant under the symmetry group $\{I, \sigma_{zc}, \pi_x, \rho_{xzc}\}$, whereas for off-critical compositions group is reduced to $\{I, \sigma_{zc}\}$.

The energy of the $(0, 1/2)$ branch is lower than the one of the homogeneous state, and larger than the one of the laterally structured branch $(1/2, 0)$ that also has a single but much shorter diffuse interface. As for the rest of the branches there is a slow monotonous decrease of the energy with $\bar{c}$ for the reasons outlined in Sect. 4.1

4.3 Checkerboard films

Up to here, we have studied branches that show at $\bar{c} = 0$ purely lateral or vertical structuring, and the changes along the branches (and emerging side-branches) that

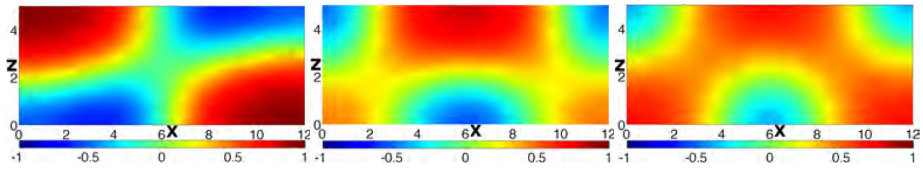

Fig. 5. Typical concentration profiles on (a) the checkerboard branch $(1/2, 1/2)$ at the label n in Fig. 1(a), (b) the checkerboard branch $(1, 1/2)$ at label u in Fig. 1(a), and (c) on its side-branch at label t in Fig. 1(a).

result when increasing the concentration. Another type of profile found at $\bar{c} = 0$ corresponds to a 'superposition' of lateral and vertical structuring giving rise to checkerboard states. In particular, for $\bar{c} = 0$ the condition $k_x^2 + k_y^2 < 1$ must be satisfied as discussed in the section on linear stability. Thus the only possible branches for $H = 5$ and $L = 12$ are $(1/2, 1/2)$ and $(1, 1/2)$. These are the checkerboard films we find numerically (see heavy dash-dash-dotted lines in Fig. 1). They only exist well within the spinodal region.

A typical profile on the $(1/2, 1/2)$ branch is shown in Fig. 5(a). At $\bar{c} = 0$ this branch is invariant under the symmetry group $\{I, \pi_x, \pi_z, \pi_c\}$ while at $\bar{c} \neq 0$ the group is $\{I, \pi_c\}$. A typical profile on the $(1, 1/2)$ branch is shown in Fig. 5(b). At $\bar{c} = 0$ this branch is invariant under $\{I, \sigma_{zc}, \pi_x, \rho_{xyz}\}$ while at $\bar{c} \neq 0$ the group is $\{I, \sigma_{zc}\}$. At $\bar{c} = 0.13$ a side-branch emerges that always has a higher L_2 norm than the $(1, 1/2)$ branch itself. On the side-branch when one increases $\bar{c}$ the horizontal and vertical interfaces transform to parts of circular arcs that limit a droplet on the centre of the substrate, and another two in the upper left and right corner, respectively (cf. Fig. 5(c)).

With increasing $\bar{c}$ both checkerboard states widen their diffuse interfaces until merging with the homogeneous states $(0, 0)$ through pitchfork bifurcations at $\bar{c}_{1/2,1/2} = 0.42$ for $(1/2, 1/2)$ and $\bar{c}_{1,1/2} = 0.33$ for $(1, 1/2)$, as also obtained from Eq. (2) setting the corresponding vertical n and horizontal s mode numbers.

The checkerboard films are lower energetically than the homogeneous state in Fig. 1(b). The film with more internal interfaces $(1, 1/2)$ is of larger energy than the $(1/2, 1/2)$ film. Both are energetically more expensive than purely vertically or laterally structured films due the greater overall length of internal diffuse interfaces.

4.4 Oblique films

In contrast to the films discussed above that exist at $\bar{c} = 0$, the oblique films do not emerge from the trivial state as described by Eq. (2) for some combination of mode numbers. Instead they emerge from laterally structured $(s, 0)$ or layered films $(0, n)$ in symmetry breaking pitchfork bifurcations when changing the domain size (cf. Fig. 8 of Ref. [10]). Here we find that they also join laterally structured or layered films at some off-critical composition.

The branch O_1 emerges in the critical case from the branch $(1, 0)$ and here joins the layered state $(0, 1/2)$ at $\bar{c} = 0.27$. A profile from the O_1 branch is presented in Fig. 6(a). As $\bar{c}$ is increased the bend in the diffuse interface becomes weaker before it becomes horizontal where it joins the branch $(0, 1/2)$. This branch is always invariant under $\{I, \sigma_{zc}\}$.

The branch $O_{3/2}$ emerges in the critical case from the branch $(3/2, 0)$ and here joins the same branch at the small off-critical composition $\bar{c} = 0.09$. Figure 6(b) shows a profile from this branch, the similarity with profiles on the $(3/2, 0)$ branch

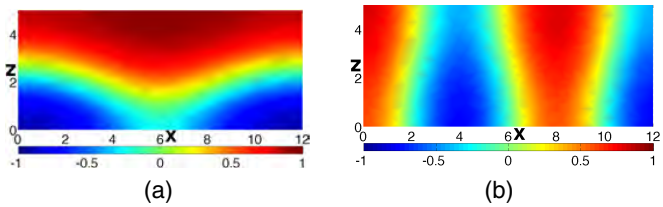

Fig. 6. Typical concentration profiles on (a) the oblique branch O_1 at label k in Fig. 1(a) and (b) the oblique branch $O_{3/2}$ at label r in Fig. 1(a).

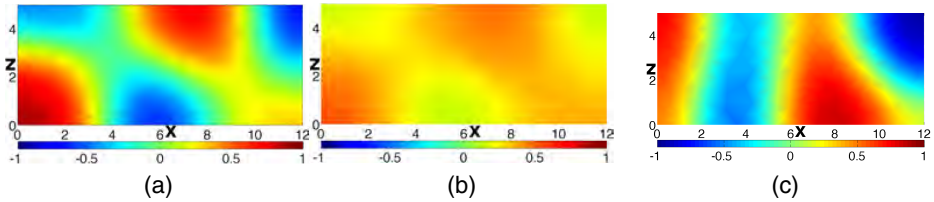

Fig. 7. Typical concentration profiles on branch $J^{1,1/2}_{3/2}$ at (a) point v and (b) point w in Fig. 1(a), and (c) of branch $J^{1/2,1/2}_{3/2}$ at s

is evident. At $\bar{c} = 0$ this branch is invariant under the symmetry group $\{I, \rho_{xyz}\}$, reduced in the off-critical case to $\{I\}$.

The O_1 films have a long bended diffuse interface, while the $O_{3/2}$ films exhibit three shorter inclined vertical ones. The analysis of the energy of this states in Fig. 1(b) shows that the total cost of producing the latter is larger.

4.5 Oblique checkerboard films

Next we discuss another type of films that can be seen as a type of checkerboard films with inclined interfaces. These films are located on the branches $J^{1,1/2}_{3/2,0}$ and $J^{1/2,1/2}_{3/2,0}$ in Fig. 1.

When changing L at $\bar{c} = 0$ the branch $J^{1,1/2}_{3/2,0}$ joins the laterally stratified $(3/2, 0)$ branch with the checkerboard $(1, 1/2)$ branch, and $J^{1/2,1/2}_{3/2,0}$ joins the laterally stratified $(3/2, 0)$ branch with the checkerboard $(1/2, 1/2)$ (cf. Fig. 8 of Ref. [10]). This implies that along its length the mode numbers in horizontal and vertical direction are changed through continuous bending and reconnection of diffuse interfaces. Along the branch $J^{1,1/2}_{3/2,0}$ the L_2 norm decreases monotonously up to $\bar{c} = 0.32$, beyond this point our numerics is not able to follow this branch. Two typical profiles from this branch are shown in Figs. 7(a) and 7(b), where the progressive widening and dilution of the interfaces with increasing $\bar{c}$ is clearly observed. At $\bar{c} = 0$ the branch $J^{1,1/2}_{3/2,0}$ is invariant under $\{I, \rho_{xzc}\}$, and for $\bar{c} \neq 0$ only under $\{I\}$.

The branch $J^{1/2,1/2}_{3/2,0}$ exists for a small range of off-critical compositions, merging with $(3/2, 0)$ at $\bar{c} = 0.14$. As shown in Fig. 7(c), when $\bar{c}$ increases the lower part of the diffuse interface at the right shifts from the right wall towards the substrate, leading finally to the lateral structuring typical of $(3/2, 0)$.

Apart from the homogeneous state, the energy on these branches is only lower than that of the checkerboard states because the diffuse interfaces have steeper gradients in the latter.

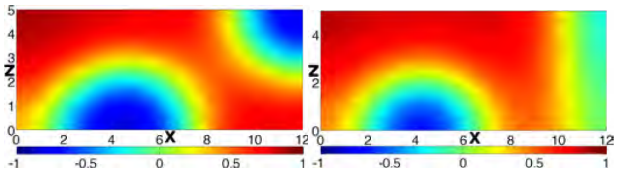

Fig. 8. Typical concentration profiles on branch $C_{1/2}^{1/2}$ on (a) the lower and (b) upper sub-branch labeled by m and l in Fig. 1(a), respectively.

4.6 Droplets and stripes

The final solutions we discuss are the ones on the branches $C_{1/2}^{1/2}$. These are two sub-branch that both seem to emerge at $\bar{c} = 0.16$ from the branch $(1/2, 1/2)$. They only exist at off-critical compositions. As observed in the profile from the lower sub-branch (cf. Fig. 8(a)) it evolves from a profile on the branch $(1/2, 1/2)$ by inclining the left horizontal interface towards the substrate and detaching of component 2 (blue online) from the left lower corner, giving rise to the formation of a droplet of component 2 deposited on the lower substrate. At the top right corner another droplet of component 2 develops. Moving along the lower sub-branch with increasing $\bar{c}$ the droplet at the top right corner gets progressively squeezed against the right boundary creating a vertical stripe, that coexists with the droplet on the substrate. One could call this a reverse Plateau Rayleigh transition.

Note that this branch is only invariant under the identity transformation I, showing once more how off-critical compositions easily break all the symmetries. This branch is on the L_2 diagram situated between the O_1 and $(1/2, 1/2)$ branches, and its energy is also bounded by the energy of these branches.

5 Conclusions

We have presented two-dimensional steady morphologies for flat films of a binary mixture that is confined into a rectangular geometry (film thickness $H = 5$ and lateral extension $L = 12$). A high surface tension imposes a flat free surface. The obtained 2D concentration profiles correspond to steady solutions of the Cahn-Hilliard equation in a rectangular domain at off-critical compositions. The solutions are obtained through a minimisation of the underlying Lyapunov functional using a gradient method. The present consideration of a rectangular geometry without energetic bias and flat free surface in the off-critical case will serve as a reference case for a future study of the off-critical case with energetic bias at the free surface and with modulated free surface.

We have obtained the bifurcation diagram with the mean concentration as control parameter and the L_2 norm of the concentration field and energy as solution measures. A linear stability analysis has established the region of linear instability (spinodal region) where the homogeneous film is unstable to at least one instability mode. Within the spinodal region laterally structured films of type $(1/2, 0)$ are stable and have minimal energy. For the presented geometry there exist several primary bifurcation from the homogeneous state. They are all pitchfork bifurcations whose loci may be calculated analytically through the linear analysis.

We have numerically determined and briefly discussed solutions of various types: laterally structured films, stratified layers, checkerboard films, oblique films, films

with several droplets and films with droplets and stripes. Thereby, some of the solutions, like the films with droplets and stripes, only exist for off-critical compositions. Note that part of the results are similar to results recently obtained on the square domain [18]. However, as the rectangular domain is less symmetric than the square domain, here several of the degeneracies between solution branches are lifted (e.g., the one between laterally structured and stratified films) and the obtained bifurcation diagram is more involved.

F. A. M. Bribesh acknowledges support by the Libyan Ministry of Higher Education. S. Madruga acknowledges the EU via a FP7 Marie Curie Reintegration Grant (PERG04-GA-2008-234384), the *Fundación Caja Madrid* via *Becas de Movilidad para Profesores 2011-2012* program, the Spanish *Ministerio de Ciencia e Innovación* via the project TRA2010-18054, and the Department for Mathematical Sciences at Loughborough University for hosting him for this study.

References

1. M. Geoghegan, G. Krausch, Prog. Polym. Sci. **28**, 261 (2003)
2. J.W. Cahn, J.E. Hilliard, J. Chem. Phys. **28**, 258 (1958)
3. J.W. Cahn, J. Chem. Phys. **42**, 93 (1965)
4. D.M. Anderson, G.B. McFadden, A.A. Wheeler, Ann. Rev. Fluid Mech. **30** 139 (1998)
5. H.P. Fischer, P. Maass, W. Dieterich, Phys. Rev. Lett. **79**, 893 (1997)
6. R. Kenzler, F. Eurich, P. Maass, B. Rinn, J. Schropp, E. Bohl, W. Dieterich, Comp. Phys. Comm. **133**, 139 (2001)
7. O.A. Frolovskaya, A.A. Nepomnyashchy, A. Oron, A.A. Golovin, Phys. Fluids **20**, 112105 (2008)
8. U. Thiele, S. Madruga, L. Frastia, Phys. Fluids **19**, 122106 (2007)
9. S. Madruga, U. Thiele, Phys. Fluids **21**, 062104 (2009)
10. F.A.M. Bribesh, L. Frastia, U. Thiele, Phys. Fluids **24**, 062109 (2012)
11. A. Novick-Cohen, L.A. Segel, Physica D **10**, 277 (1984)
12. A. Novick-Cohen, J. Stat. Phys. **38**, 707 (1985)
13. P.C. Fife, B. Kielhofer, S. Maier-Paape, T. Wanner, Physica D **100**, 257 (1997)
14. H. Kielhofer, Proceedings Of The Royal Society Of Edinburgh Section A-Mathematics **127**, 1219 (1997)
15. H. Kielhofer, Arch. Rational Mech. Anal. **155**, 261 (2000)
16. T.J. Healey, H. Kielhöfer, Siam J. Math. Anal. **31**, 1307 (2000)
17. S. Maier-Paape, K. Mischaikow, T. Wanner, Inter. J. Bifur. Chaos **17**, 1221 (2007)
18. S. Maier-Paape, U. Miller, K. Mischaikow, T. Wanner, Rev. Mat. Complut. **21**, 351 (2008)
19. L. Frastia, U. Thiele, L.M. Pismen, Math. Model. Nat. Phenom. **6**, 62 (2011)